Nanoscale Research Letters

NANO EXPRESS

Open Access

Graphene-Based Polarization-Independent Mid-Infrared Electro-Absorption Modulator Integrated in a Chalcogenide Glass Waveguide

Yong Zhou[1], Rongguo Lu[1*], Guangbiao Wang[1], Jiangbo Lyu[1], Meng Tan[1], Liming Shen[1], Rui Lin[1], Zhonghua Yang[2] and Yong Liu[1]

Abstract

A polarization-insensitive graphene-based mid-infrared optical modulator is presented that comprised SiO_2/$Ge_{23}Sb_7S_{70}$, in which two graphene layers are embedded with a semiellipse layout to support transverse magnetic (TM) and transverse electric (TE) polarizing modes with identical absorption. The key performance index for the polarization independent modulator is polarization-sensitivity loss (PSL). The waveguide of our device just supports basic TE and TM modes, and the PSL between two modes is of < 0.24 dB. The model can offer extinction ratio (ER) more than 16 dB and insertion loss less than 1 dB. The operation spectrum ranges from 2 to 2.4 μm with optical bandwidth of 400 nm. The 3 dB modulation bandwidth is as high as 136 GHz based on theoretical calculation.

Keywords: Chalcogenide glass, Graphene, Mid-infrared, Optical-modulator, Polarization-insensitive

Introduction

Near-infrared wavelength optical fiber communication networks are becoming the core of the whole telecommunication networks. However, the mid-infrared is also an important waveband for the application of electro-optic device in military and civil fields, such as infrared countermeasure, chemical sensing, infrared guidance, environmental monitoring, space communication, etc. In addition, mid-infrared integrated electro-optic devices, such as photodetectors and modulators, also are developed to expand the 1.55 μm communication window.

In recent years, 2D functional electro-optic materials, such as graphene [1–4], chalcogenide [5], and black phosphorus [6], have been discovered, which accelerated the development of integrated electro-optic and broke the traditional performance limitation. Among these materials, graphene is considered as an ideal material for realizing optical modulators due to some attractive advantages [7], such as constant absorption over a wide spectrum [8], ultra-high carrier mobility at room temperature [9], electrically controllable conductivity and compatibility with CMOS processing. Consequently, graphene-based optical modulator has become a hot research topic. However, by far, the operation waveband of most reported graphene-based optical modulators is around 1.31 μm or 1.55 μm [10–13]. The modulation principle of near infrared and mid-infrared is the same, but the operation wavelength of modulator mainly depends on the waveguide transparency windows. The key point for the realization of graphene-based mid-infrared modulators is the integration of graphene and various mid-infrared waveguide materials. In 2017, Lin et al. [14] reported a mid-infrared electro-absorption optical modulator based on $Ge_{23}Sb_7S_{70}$-on-graphene structure, which opened the field of graphene-based mid-infrared modulator.

Graphene as electro-optic material, we also need to consider one of the most important characteristics of anisotropic dielectric [15], which has been experimentally

*Correspondence: lurongguo@uestc.edu.cn
[1] School of Optoelectronic Science and Engineering, University of Electronic Science and Technology of China, Chengdu 610054, China
Full list of author information is available at the end of the article

proved in this article [16]. The permittivity in plane is tunable, however, the permittivity in vertical is a constant of 2.5. So, the graphene can only strongly interact with the in-plane electric field [10], that is the reason why reported graphene-based modulators before have a strong polarization dependence, in which modulators can only modulate in-plane electric filed mode [10–13]. Generally, the polarization state of light in waveguide or fiber is random. To realize the wide commercial application of graphene-based modulator, the problem of polarization dependent needs to be solved.

In this work, we present a new structure of graphene-based mid-infrared polarization-independent electro-optic modulator, which has the advantages of large modulation bandwidth and wide spectrum of polarization insensitivity. We used the SOI structure and a $Ge_{23}Sb_7S_{70}$ glass strip which is embedded in SiO_2 cladding as waveguide core. In the $Ge_{23}Sb_7S_{70}$ waveguide, two graphene layers are U (semiellipse)-type distribution and are insulated by $Ge_{23}Sb_7S_{70}$ glass. Since the graphene layer is U-type distribution, both TE and TM modes can strongly interact with graphene. By proper choosing structure parameters, we can well overcome the polarization dependence. Using the finite element method (FEM), we analyzed the effective mode index (EMI) and absorption coefficient (α) of the *U*-structure device. The result shows that the real parts of EMI for TE (N_{te}) and TM (N_{tm}) modes have the same fluctuations (with constant difference) in different chemical potential (μ_c), and the imaginary parts of both TE and TM modes have almost identical fluctuations and wavelength independent in a wide spectrum. By proper choosing of switching points for "ON" and "OFF" states, for both TE and TM modes, the modulation depth is more than 16 dB, the operation wavelength spectrum is 2–2.4 μm, the PSL is less than 0.24 dB, and the theoretical 3 dB modulation bandwidth is as high as 136 GHz.

Methods

The transparency window of $Ge_{23}Sb_7S_{70}$ glass ranges from 2 to 10 μm [17] that is a great material for mid-infrared photonics. Previous study led by Lin et al. [14] has proved its feasibility to realize $Ge_{23}Sb_7S_{70}$-graphene mid-infrared modulator. In this work, we also take $Ge_{23}Sb_7S_{70}$ glass as waveguide material. The geometrical structure of our proposed modulator is depicted in Fig. 1, which was fabricated using a thermal nanoimprint process. Details of the process steps are schematically illustrated in Fig. 1. You can also reference paper [18] to get details for the preparation of PDMS composite stamps and $Ge_{23}Sb_7S_{70}$ glass solution. Details for geometrical size and materials are presented in Fig. 2b.

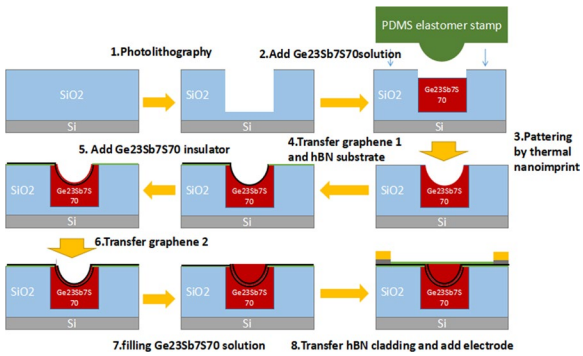

Fig. 1 Schematic process flow of the graphene-based modulator integrated in $Ge_{23}Sb_7S_{70}$

A SiO_2 layer with thickness h = 0.8 μm was grown on Si substrate, and then a groove with width w = 0.96 μm and height h = 0.8 μm was made in SiO_2 layer by using photolithography method. After filling $Ge_{23}Sb_7S_{70}$ solution and pattering by thermal nanoimprint, a U-type $Ge_{23}Sb_7S_{70}$ groove was made. A 10-nm-thickness hexagonal boron nitride (hBN) layer was paved at flat area. Then, first graphene layer, 50-nm-thickness (spin-coating) $Ge_{23}Sb_7S_{70}$ insulator and second graphene layer were paved to the U-type $Ge_{23}Sb_7S_{70}$ groove in order. Finally, we filled the U-type $Ge_{23}Sb_7S_{70}$ groove with $Ge_{23}Sb_7S_{70}$ solution and transferred hBN cladding and added electrode. The electrode structure is Au–Pd-graphene since the contact resistance between graphene and Pd is less than 100(Ω/μm) [19]. Graphene sheet width between electrode and waveguide is 0.8 μm. Figure 2c, d presents the electric field distribution for both TE (in-plane) and TM (vertical-plane) modes.

When voltage is applied onto the graphene, graphene's chemical potential μ_c is dynamically tuned. In our model, graphene is treated as an anisotropic material. The perpendicular permittivity $\varepsilon_\perp$ of the graphene does not vary with the μ_c and always stays as a constant of 2.5, whereas the in-plane permittivity of the graphene $\varepsilon_\parallel$ can be tuned as [12].

$$\varepsilon_\parallel(\omega) = 1 + \frac{i\delta}{\omega\varepsilon_0 h_g} \tag{1}$$

The δ stands for the conductivity of graphene and relates to chemical potential μ_c, which can be deduced from Kubo formula [20]. The ω represents the radian frequency, and h_g = 0.7 nm is the effective thickness of graphene.

We made a $Ge_{23}Sb_7S_{70}$ strip waveguide, in which two flat graphene layers were embedded (Fig. 3 insert). Figure 3 plots the real and imaginary part of EMI for both TE and TM mode at the wavelength of 2.2 μm. The

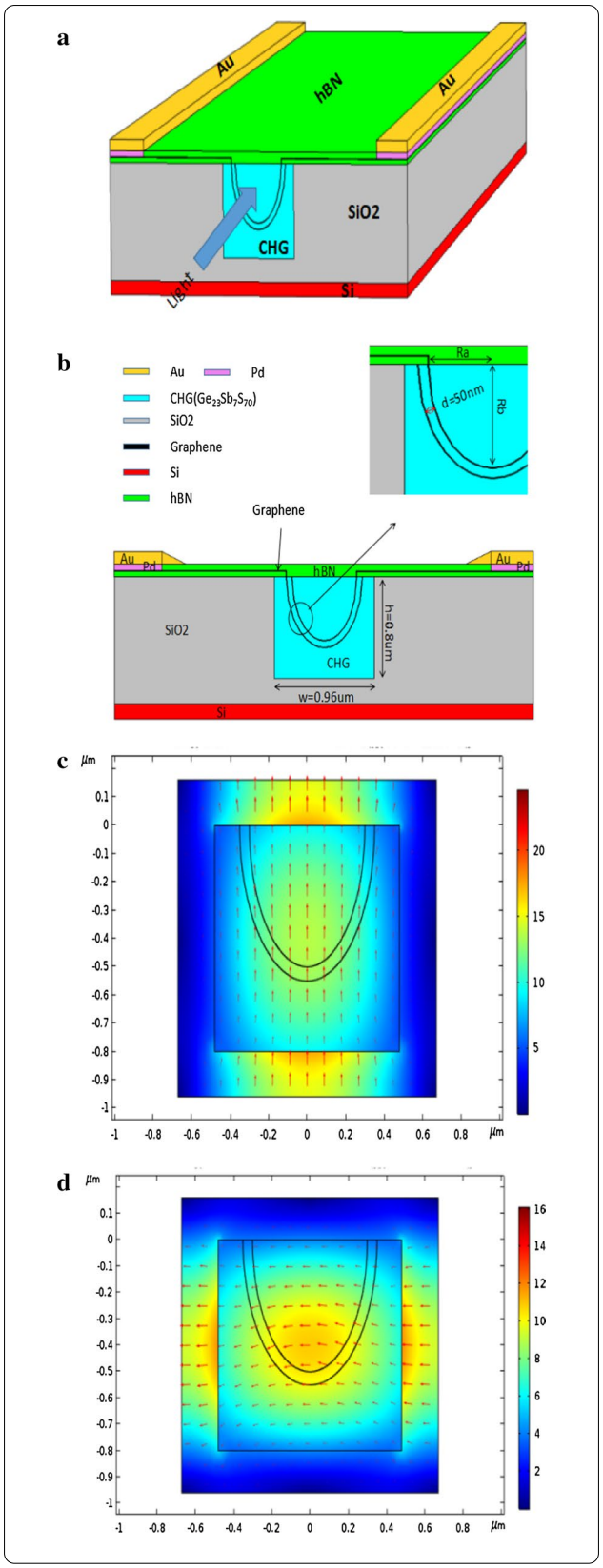

Fig. 2 Illustration of the polarization-independent electro-absorption optical modulator. **a** 3D Schematic diagram of the modulator; **b** 2D cross section of the U-structure $Ge_{23}Sb_7S_{70}$-graphene waveguide, distance between two graphene layer $d = 50$ nm, waveguide width $w = 0.96$ μm, height $h = 0.8$ μm. The electric field distribution for TE mode (**c**) and TM mode (**d**), arrows indicate the direction of polarization

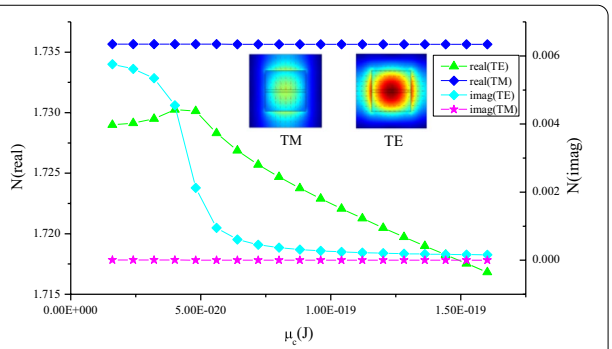

Fig. 3 Graphene was straightly paved in $Ge_{23}Sb_7S_{70}$ strip waveguide. The real and imaginary parts of EMI for both TE and TM modes at the wavelength of 2.2 μm

EMI of TE mode changed obviously for both real and imaginary parts. On contrary, no significant fluctuations occurred to the EMI of TM mode for both real and imaginary parts. The main reason is that TM mode polarization is perpendicular to the graphene plane and $\varepsilon_{\|}$ is nontunable in chemical potential. In this work, we bend the graphene layer as U-type layout to impose equal influence on both TE and TM modes.

Results and Discussion

Although the polarization-independent electro-optic modulator based on graphene has been reported [15–21], the polarization independence of these devices is closely related to wavelength [22]. Therefore, in our model, the U-structure is used, in which we find that the sensitivity of the waveguide polarization is weak correlation with wavelength. The imaginary part of the EMI is known as electro-absorption. As shown in Fig. 3, the imaginary part of the EMI reaches peak at low chemical potential around $\mu_c = 0.1$ eV. Thus, the $\mu_c = 0.1$ eV point can be chosen as "OFF" state point. At the same time, the discrepancy of imaginary part of the EMI between TE and TM modes is highest at "OFF" state point. To get lower discrepancy of absorption, we just need to minimize the discrepancy of absorption at "OFF" state point. At wavelength = 2.2 μm and Ra = 0.35 μm (size of minor radius of the ellipse

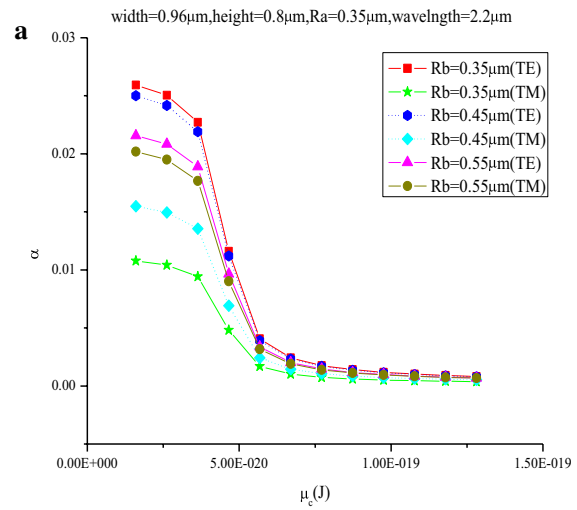

Fig. 4 **a** Absorption coefficient of TE and TM modes as a function of μ_c at different Rb, (wavelength = 2.2 μm, Ra = 0.35 μm); **b** the absorption coefficient of TE and TM modes as a function of Rb (Ra = 0.35 μm, wavelength = 2.2 μm, μ_c = 0.1 eV)

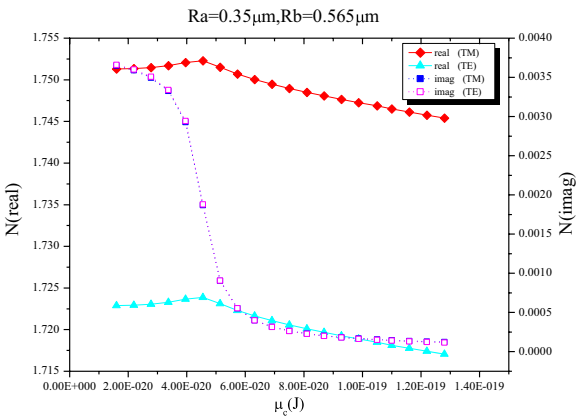

Fig. 5 Illustration of the real and imaginary parts of EMI for both TE and TM modes as a function of chemical potential

that is the horizontal axis), by sweeping the μ_c from 0.1 to 0.8 eV, under different Rb (size of major radius of the ellipse that is the vertical axis), the influence of varied μ_c on EMI for both TE and TM modes is analyzed, as shown in Fig. 4a. It is obvious that the discrepancy values between the TE and TM modes decrease rapidly as Rb is tuned from 0.35 to 0.55 μm. It indicates that it is possible to reach lower PSL around Rb = 0.55um. Therefore, sweeping the parameter Rb around 0.55 μm, we find that the discrepancy of absorption between TE and TM modes decreases firstly and then increases with the increase in Rb. At the point Rb = 0.565 μm, a minimum value can be obtained.

When Ra = 0.35 μm, Rb = 0.565 μm, wavelength = 2.2 μm, the variation of EMI for both TE and TM modes with chemical potential was analyzed. As shown in Fig. 5, the real part of EMI has same variation trend for TE and TM modes with constant difference. Since the modulator is based on electro-absorption principle, we just need to care about the imaginary part of EMI. What is more, under all the μ_c values, the α of both TE and TM are almost identical. It is the property that we need for designing polarization independent electro-absorption modulator. A highest and lowest value of α (proportional to the imaginary part of EMI) can be obtained at $\mu_c = 0.1$ eV and $\mu_c = 0.8$ eV, respectively (Fig. 5). Thus, the point of $\mu_c = 0.1$ eV and $\mu_c = 0.8$ eV can be chosen as "OFF" and "ON" state point.

The variation of α as a function of wavelength is presented in Fig. 6a, b. It can be seen from Fig. 6 that the α of the two modes is very identical with the wavelength change in the strong absorption state ("OFF" state), and the differences between the two modes have been kept relatively small. At the "ON" state, the discrepancy of α between TE and TM modes is at the order of 10^{-4}. To measure the discrepancy further and accurately between two modes, PSL is defined as PSL = ER(TE)-ER(TM), where ER is the extinction ratio. We measured the modulation depth of the modulator in two modes as a function of wavelength under the condition of 200 μm long waveguide. As shown in Fig. 7, it can be seen from the diagram that in a wide spectrum range of 2–2.4 μm, the modulation depth of the two modes is more than 16 dB, and PSL is less than 0.24 dB.

For an optical modulator, the 3 dB modulation bandwidth f_{3dB} is always one of the important parameters to

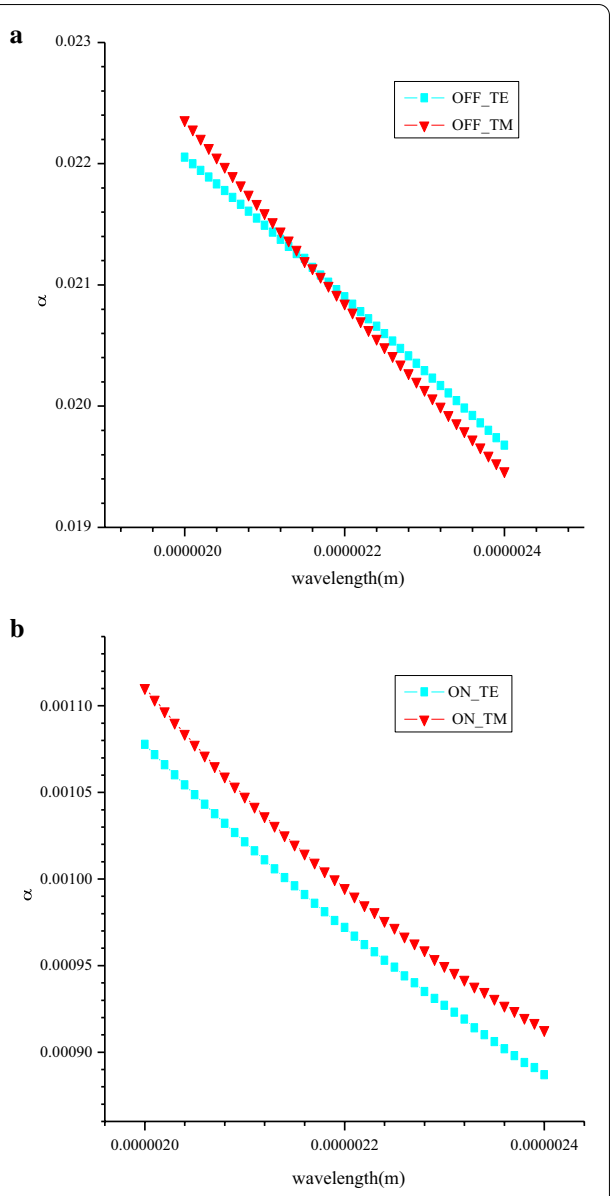

Fig. 6 Absorption coefficients (*α*) of TE and TM have an almost identical fluctuation with the change of wavelength at "OFF" state (**a**) and "ON" state (**b**)

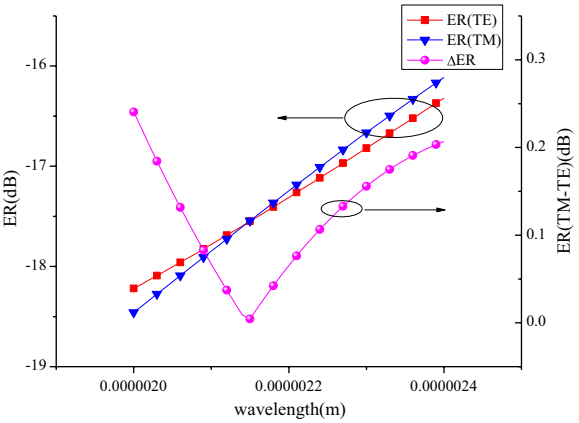

Fig. 7 Modulation depth of the two modes and PSL (line ER(TE-TM)) between two modes at different wavelengths

be concerned about. Since graphene has ultrahigh carrier mobility at room temperature, the graphene-based modulator's operation speed is no longer limited by minority carrier lifetime like traditional semiconductor modulators are. The f_{3dB} of a graphene-based modulator is mainly impeded by RC delay, which can be expressed as

$$f_{3\,\mathrm{dB}} = \frac{1}{2\pi RC} \tag{2}$$

The R is the device's total resistance, including graphene sheet resistance Rs and metal–graphene contact resistance Rc, which has been carefully discussed in previous works [23]-[25]. The C is the capacitance of modulator, which mainly consists of the capacitor that is formed by the two graphene flakes. Although this capacitor is not an ideal parallel-plate capacitor model, to preliminarily estimate the f_{3dB}, we still use the parallel-plate capacitor model to calculate the C. In our calculations, Rc = 100 Ω/μm [19] and Rs = 200 Ω/μm [26] were used, and the overlap width of two graphene flakes is about 1.53 μm. The estimated f_{3dB} is as high as 136 GHz. Moreover, lower values of both Rs and Rc are possible in the future, which means higher f_{3dB} can be obtained.

The above simulations are based on the semiellipse layout with Ra = 0.35 μm and Rb = 0.565 μm. However, in fabrication, this exact radius size cannot always be guaranteed. Therefore, we have also investigated the fabrication tolerance (Fig. 8). When Ra varies from 0.345 to 0.355 μm (Fig. 8a), or Rb varies from 0.56 to 0.57 μm (Fig. 8b), the PSL between two modes is still lower than 0.6 dB. So, our device has large fabrication tolerance.

Conclusions

In conclusion, we presented a concept of a broadband polarization-independent graphene-based mid-infrared electro-absorption optical modulator. In our structure, a U-structure double-layer graphene is placed in chalcogenide glass waveguide. Under different graphene chemical potentials, different wavelengths and different short radius lengths, the graphene-induced EMI variations for both TE and TM modes are investigated. The results show that TE and TM modes have almost identical absorption coefficient variation in the mid-infrared 2–2.4 μm, which fulfills the requirement of

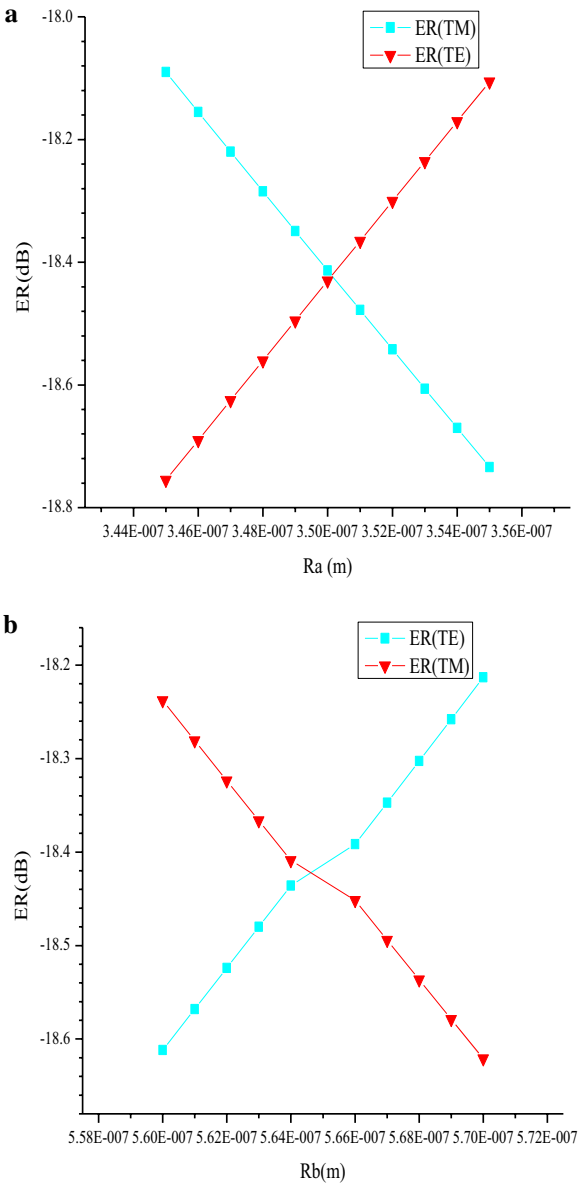

Fig. 8 Modulation depth of the two modes at different Ra (**a**) or Rb (**b**)

polarization-independent modulation. Based on this structure, the modulator with a length of 200 μm has a modulation depth more than 16 dB. The modulation depth difference between the two modes is 0.24 dB, and the theoretical modulation bandwidth of the device is as high as 136 GHz. We believe that this mid-infrared polarization-independent graphene-based electro-optic modulator will further promote the study of the graphene-based modulator in the middle-infrared bands.

Abbreviations

ER: Extinction ratio; TM: Transverse magnetic; TE: Transverse electric; PSL: Polarization-sensitivity loss; FEM: Finite element method; EMI: Effective mode index; hBN: Hexagonal boron nitride.

Acknowledgements

The authors greatly acknowledge the University of Electronic Science and Technology of China and the Chongqing United Microelectronics Center.

Authors' contributions

YZ and RL did the design. JL, MT, LS, RL and ZY did the simulation together. YZ and GW wrote the initial drafts of the work. RL and YL commented and revised on the manuscript. All authors read and approved the final manuscript.

Funding

This work was funded by National Key Research and Development Program of China (2019YFB2203800), Sichuan Science and Technology Program (2020YFH0108) and the Fundamental Research Funds for the Central Universities (ZYGX2019J046).

Availability of data and materials

All data generated or analyzed during this study are included in this published article.

Declarations

Competing interests

The authors declare that they have no competing interests.

Author details

[1]School of Optoelectronic Science and Engineering, University of Electronic Science and Technology of China, Chengdu 610054, China. [2]Chongqing United Microelectronics Center, Chongqing 401332, China.

Received: 4 March 2021 Accepted: 27 April 2021
Published online: 08 May 2021

References

1. Ferrari AC et al (2015) Science and technology roadmap for graphene, related two-dimensional crystals, and hybrid systems. Nanoscale 7(11):4598–4810
2. He X, Liu F, Lin F et al (2021) Tunable 3D Dirac-semimetals supported mid-IR hybrid plasmonic waveguides. Opt Lett 46(3):472–475
3. Peng J, He X, Shi C et al (2020) Investigation of graphene supported terahertz elliptical metamaterials. Phys E 124:114309
4. He X, Liu F, Lin F et al (2021) Tunable terahertz Dirac semimetal metamaterials. J Phys D Appl Phys 54(23):235103
5. Choi W et al (2017) Recent development of two-dimensional transition metal dichalcogenides and their applications. Mater Today 20(3):116–130
6. Ling X et al (2015) The renaissance of black phosphorus. Proc Natl Acad Sci USA 112(15):4523
7. Yu SL et al (2017) 2D Materials for optical modulation: challenges and opportunities. Adv Mater 29(14):201606128
8. Nair RR et al (2008) Fine structure constant defines visual transparency of graphene. Science 320(5881):1308–1308
9. Bolotin KI et al (2008) Ultrahigh electron mobility in suspended graphene. Solid State Commun 146(9):351–355
10. Liu M et al (2011) A graphene-based broadband optical modulator. Nature 474(7349):64–67
11. Liu M, Yin X, Zhang X (2012) Double-layer graphene optical modulator. Nano Lett 12(3):1482–1485
12. Koester SJ, Li M (2012) High-speed waveguide-coupled graphene-on-graphene optical modulators. Appl Phys Lett 100(17):611
13. Phare CT et al (2015) Graphene electro-optic modulator with 30 GHz bandwidth. Nat Photonics 9(8):511–514
14. Lin H et al (2017) Chalcogenide glass-on-graphene photonics. Nat Photonics 11(12):798–806

15. Hao R et al (2015) Graphene assisted TE/TM-independent polarizer based on Mach-Zehnder interferometer. IEEE Photonics Technol Lett 27(10):1112–1115
16. Chang Z, Chiang KS (2016) Experimental verification of optical models of graphene with multimode slab waveguides. Opt Lett 41(9):2129–2132
17. Luo Z et al (2017) Mid-infrared integrated photonics on silicon: a perspective. Nanophotonics 7(2):393–420
18. Zou Y et al (2015) Solution processing and resist-free nanoimprint fabrication of thin film chalcogenide glass devices: inorganic-organic hybrid photonic integration. Adv Opt Mater 2(8):759–764
19. Zhong H et al (2015) Realization of low contact resistance close to theoretical limit in graphene transistors. Nano Res 8(5):1669–1679
20. Falkovsky LA (2008) Optical properties of graphene. J Phys Conf 129:012004
21. Ye SW et al (2017) Polarization independent modulator by partly tilted graphene induced electro-absorption effect. IEEE Photonics Technol Lett 1(1):99
22. Hu X, Gui CC, Wang J (2014) A graphene-based polarization-insensitive optical modulator. Integr Photonics Res Silicon Nanophotonics. JT3A.25
23. Ye SW et al (2014) Electro-absorption optical modulator using dual-graphene-on-graphene configuration. Opt Exp 22(21):26173–26180
24. Koester SJ, Li M (2012) High-speed waveguide-coupled graphene-on-graphene optical modulators. Appl Phys Lett 100(21):171107
25. Bonaccorso F et al (2010) Graphene photonics and optoelectronics. Nature Photon 4(9):611–622
26. Cai WW et al (2009) Large area few-layer graphene/graphite films as transparent thin conducting electrodes. Appl Phys Lett 95(12):123115

Publisher's Note